


SCIENTIFIC REPORTS



OPEN

Full-scale experimental investigation of deposition and corrosion of pre-protector and 3rd superheater in a waste incineration plant

Wenchao Ma¹, Terrence Wenga¹, Nan Zhang², Guanyi Chen ^{1,3}, Beibei Yan¹, Zhihua Zhou¹ & Xiao Wu⁴

Municipal solid waste (MSW) incineration is widely adopted as a waste management strategy and for the energy production. However, this technology experience grave deposition and corrosion of the boiler tubes due to high chlorine (~1.09wt.%) and alkali metal (Na, K) content in MSW. Little is known about the concentration profile of these corrosive elements in the deposits at different boiler locations. Therefore, a full-scale experimental investigation was conducted to determine the concentration profile of Cl, K, Na, S, and Ca in the deposits at pre-protector and compare with those at 3rd superheater during MSW combustion at a 36 MWe waste incineration plant (WIP) in Chengdu, China. The deposit samples were analyzed using wet chemical techniques, scanning electron microscope coupled with energy dispersive spectroscopy (SEM/EDS), and X-ray diffraction (XRD). The concentrations of Na, K, and Cl were high in the deposits at pre-protector while S and Ca concentrations were high on the 3rd superheater. The pre-protector was severely corroded than the 3rd superheater. The governing mechanisms for the deposition and corrosion on these boiler locations were elucidated.

Along with the rapid population growth and industrialization, the energy demands are constantly rising, leading to the increase in fossil fuel consumption. China, one of the greatest fossil fuel consumer in the world, utilized approximately 2.7 Gt of coal in 2007 while in 2013 approximately 4.3 Gt. This immense consumption had led to the decline of fossil fuel reserves¹ and had contributed much to the incomparable environmental problems such as severe smog in China². Considering these problems, combustion of municipal solid waste (MSW) to generate electricity had gained much attention^{3,4} and can reduce the net CO₂ emission per heating value of coal and natural gas by 93% and 84% respectively⁵. The capacity of MSW incineration in China increased from 3.7 million tons in 2003 (2.5%) to 23.2 million tons in 2010 (14.7%)⁶. In 2014, there were 188 waste incineration plants (WIP) in China, running with a total combustion capacity of 1.86×10^5 tons per day (32.5%), producing 3.72 GWh electricity per day^{7,8} and the biomass power installed capacity is expected to reach 30 GW of electricity, accounting for 3% of the total installed capacity in 2020⁹.

However, combustion of MSW, which has a high concentration of Cl (0.45–0.72wt.%)¹⁰, (0.5–1.00wt.%)¹¹ and alkali metals (K and Na) result in severe ash deposition and corrosion of the boiler tubes^{11–16}. It is estimated that deposition and corrosion of the heat transfer surfaces in WIP result in reducing electricity generation by approximately 0.5–1.5%¹⁷.

Up to date, studies have been focused on the bottom ash, fly ash, deposits, and corrosion of the superheater only in MSW incinerators^{16,18,19} while other boiler parts received little attention. A previous study by Chen *et al.*²⁰ found that the elemental composition of the deposits in different parts of the boiler varies due to the changes in

¹Tianjin Engineering Center of Biomass-derived gas/oil Technology/State Key Laboratory of Engine, School of Environmental Science and Engineering, Tianjin University, Tianjin, 300072, China. ²China Construction Engineering Design Group Corporation Limited (Headquarter), Beijing, 100037, China. ³School of Science, Tibet University, Lhasa, 850012, China. ⁴China National Environmental Protection Corporation, Beijing, 100082, China. Correspondence and requests for materials should be addressed to W.M. (email: mawc916@tju.edu.cn) or G.C. (email: chen@tju.edu.cn)

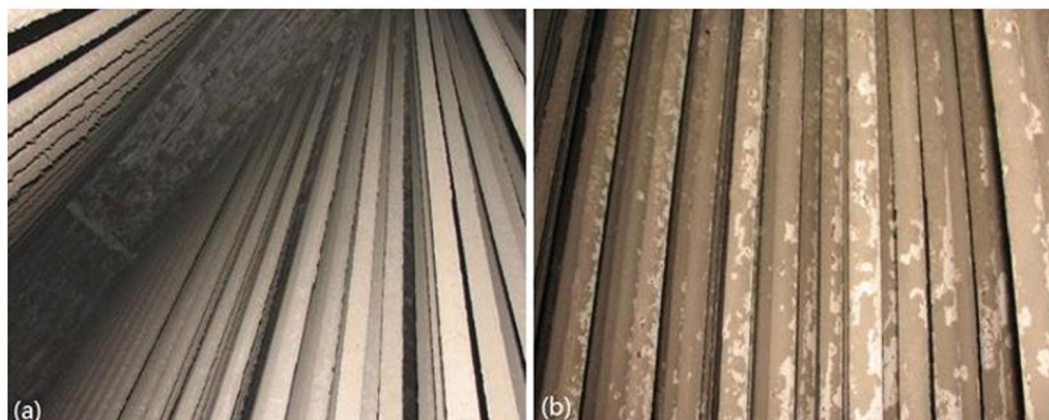


Figure 1. Ash deposits on (a) pre-protector and (b) 3rd superheater.

flue gas temperature and hence the governing mechanisms are not the same²¹. Currently, studies have reported that flue gas from the combustion chamber has a large amount of fly ash, consisting of particles ranging from submicron to millimeter¹⁹. They contain alkalis which act as glue for the secondary deposition that consists of matrixes of anhydrite calcium phase (CaSO_4), where silicates, sulfates, chlorides, and oxides are incorporated as solid particles derived from the combustion chamber²¹. These compounds undergo several physical and chemical reactions and eventually build up the deposits on the surfaces of the tubes through thermophoresis and turbulent diffusion¹². Within the deposits, mineralogical reactions between the chlorides, sulfates and the flue gas take place. Coarse fly ash particles then adhere to the initial sticky layer on the surfaces of the boiler¹⁹. Moreover, heavy metal chlorides in the deposits, as low-melting compounds, lead to a decrease of the first melting temperature of the ash deposits down to 200 °C–300 °C²², and subsequently cause dramatic corrosion on steel surfaces due to the increased chemical reactions as well as providing an electrolyte for transport of ions and chemical attack⁵.

According to Pfrang-Stotz *et al.*²³, the deposits from a WIP comprises largely of various sulfates of Ca, Na, K, Pb, and Zn with small contents of oxides, silicates, chlorides, and phosphates^{19,24}. This mineralogical composition of the deposits changes with location in the same boiler and in different types of boilers as deposition is influenced by several factors including, feedstock, type and geometry of the boiler, flue gas velocity, and temperature²¹. Changes in the deposits composition have different influences on the boiler tube corrosion.

Although extensive research on deposition and corrosion in WIP has been published, no data have been reported on the concentration profile of Na, K, Cl, Ca, and S in the deposits at pre-protector in WIP. Ash deposition and corrosion of WIP in Chengdu, China was studied. To our knowledge, high temperature corrosion usually occurred at 3rd superheater area. However, in the Chengdu waste incineration plant, the boiler actually had suffered from severe corrosion at the pre-protector. As a result, a need was identified to study the deposit chemistry on the pre-protector and compare with those on the 3rd superheater which most studies had put much focus on. The objectives of this study were to determine the amount of corrosive species in the deposits of these two heat exchangers, evaluate and compare relative severity to high temperature corrosion. The research consists of investigating the surface morphology, elemental composition and concentration distribution in the deposits. The information is useful in applying optimum corrosion measures and optimization of the combustion environment thus helps in alleviating deposition and corrosion in WIP.

Results

Morphological SEM analysis. Large amounts of deposits were formed on the pre-protector and the 3rd superheater as shown in Fig. 1. The ash deposit layer on the pre-protector was much thicker and denser than on the 3rd superheater.

The ash deposits on the 3rd superheater, in the brownish color, were thinner and some of them peeled off from the tube surface, indicating that severe corrosion had occurred. Figure 2 shows the SEM microstructure of the ash deposits at the pre-protector and the 3rd superheater. All ash deposit particles in the two pictures were in random-sizes and irregular shapes with no obvious tendency of aggregation. The particles were of different kinds of shapes including elongated, spherical, cube-like, plate-shaped and hemispherical. This observation is in line with previous studies^{25,26}.

In order to detect the morphology of the deposit particles in terms of deposit growth, the ash deposits on the pre-protector were collected and were classified into the outer, the inner and the interface layer. SEM was conducted and it was visible that three layers had different microstructures as shown in Fig. 3. The outer deposit layer had some particles in the shape of sticks, while the inner deposit layer had leaf-like shaped particles with holes accumulating together and the interface deposit layer had angular shaped and individual particles.

Chemical analysis by EDS. The chemical composition of the deposits from the pre-protector and the 3rd superheater was determined using the EDS technique. The analysis showed that sulfur was dominant in both locations. In addition, the deposits on the 3rd superheater had more Ca as the major element while the pre-protector had Na, K, and Cl as the core elements (see Fig. 4). Magnesium, silicon, and aluminum were detected in small amounts at both locations.

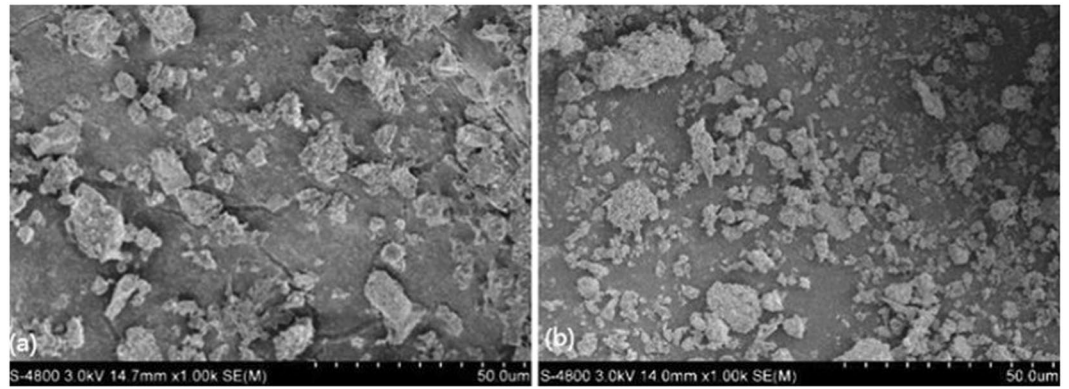


Figure 2. SEM images of deposits on (a) pre-protector and (b) 3rd superheater.

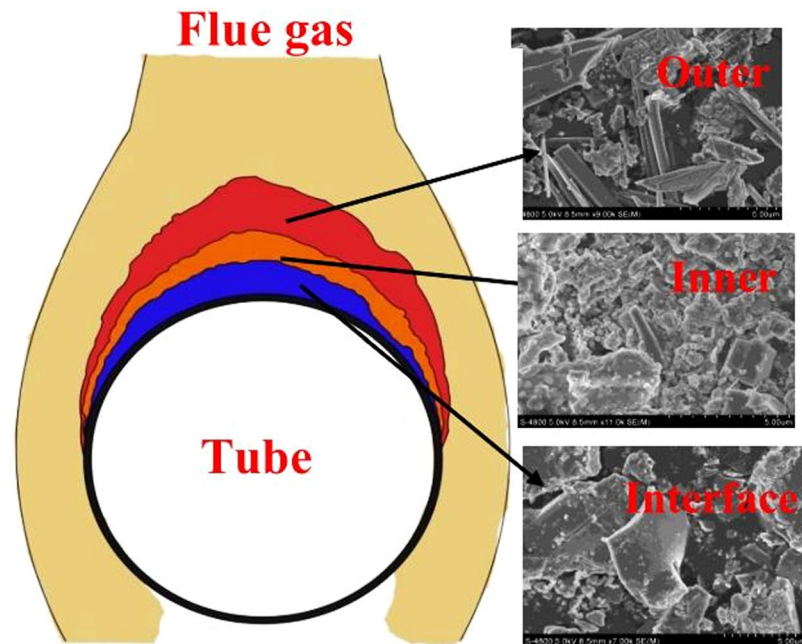


Figure 3. SEM micrograph of deposits on pre-protector in terms of growth.

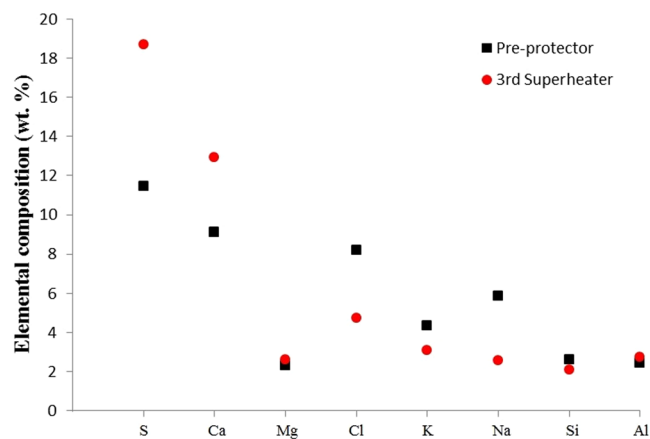


Figure 4. Elemental analysis of ash deposits on pre-protector and 3rd superheater.

Position	Major element
Outer	Cl (7.82%), Ca (8.13%), Si (2.25%), Al (3.29%), S (10.5%)
Inner	Ca (6.32%), Cl (5.58%), Na (5.89%), S (10.01%), Si (4.35%), K (4.93%)
Interface	Na (7.54%), S (14.63%), K (6.15%), Cl (1.36%)

Table 1. Elemental analysis of deposits of pre-protector in terms of growth.

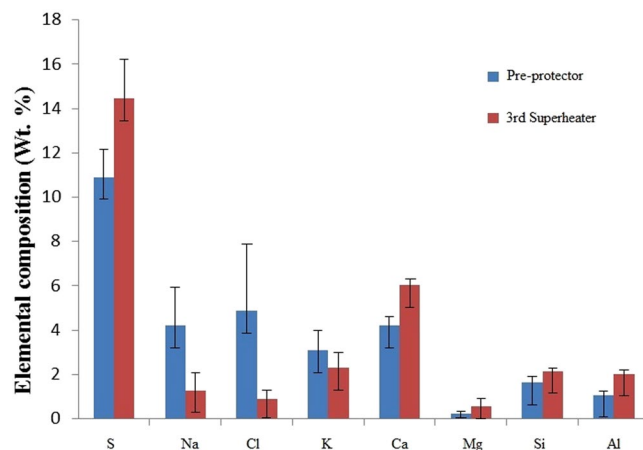


Figure 5. Elemental composition of deposits from pre-protector and 3rd superheater by wet chemical analysis.

Wet chemical analysis. The chemical composition of each deposit layer (outer, inner and interface) of the pre-protector was analyzed by a comprehensive wet chemical analysis method which takes into account large area and different particle sizes as discussed later. The concentrations of these elements are presented in Table 1.

The elements detected in the interface layer are K, Cl, Na, and S which could be KCl, NaCl, and K₂SO₄. The co-existence of alkali chlorides and sulfates in the interface of the deposits results in the formation of eutectic compounds of low melting point²⁷ which melt at low temperatures and cause corrosion by forming a flux with the protective oxide layer as well as providing a liquid phase for ionic charge transfer and for electrochemical attack, therefore, the interface layer plays a major role in accelerating corrosion as well as the medium for the exchange of ions between the metal substrate and the deposits. In addition, the eutectic low melting compounds of KCl-K₂SO₄ are sticky and can trap the coarse ash particles mainly containing silicon and calcium and this further promotes the development of the deposit. This is the reason why the inner layer contains a considerable amount of quartz and calcium sulfates (see Table 1). This observation is in good agreement with Niu *et al.*²⁸. The holes accumulating together in the inner layer presumably were due to silica and calcium sulfate particles. These particles are slow to fuse or sinter in the deposit, so they contribute to both the granular/porous nature of the deposit²⁹ and make the inner and the outer deposit layers permeable to the combustion gases to penetrate to the interface layer³⁰, thus permitting the continuation of chlorination of transition metals at the interface.

Since the sample of each layer was a mixed portion of three subsamples, the data was not used for the calculation of the overall deposit concentration because the standard deviation could not be computed from mixed samples. Therefore, in order to find the overall chemical composition of the whole deposit layer, resampling of individual samples were conducted. Five individual ash samples from randomly selected areas with varying depth from the outer surface to the interface were collected and subjected to wet chemical analysis and the results are presented in Fig. 5. The results show that the concentrations of Na and Cl were higher on the pre-protector than on the 3rd superheater while the concentration of S and Ca were higher on the 3rd superheater than the pre-protector. The error bars for S, Ca, Cl, and Na do not overlap; therefore, there is a significant difference in concentration between the pre-protector and the 3rd superheater. The measurement uncertainties represented by error bars (standard deviation) on both locations were approximately similar, but the deviation between the average values and the standard deviation are much larger for Cl on the pre-protector. This observation can be attributed to the different composition and concentrations of the elements in particles in the deposits. At the surface, the deposits are dominated by irregularly shaped particles with more rod-shaped, which had a high content of chlorine and sodium while in the inner layer; particles rich in Si and S were dominant resulting in a considerable deviation for Cl.

During the flight of the flue gas from the combustion chamber to the convective section, flue gas temperature decreases and the volatile alkali chlorides condense. The vapor-condensation of alkali chlorides (NaCl and KCl) from the flue gas at 700 °C is higher than the flue gas at 550 °C³¹. Since the flue gas temperature at the pre-protector is around 700 °C, condensation of alkali chloride might have occurred at the pre-protector than at the 3rd superheater where the temperature is around 500 °C. This might explain the occurrence of more amounts of Na and Cl on the pre-protector than on the 3rd superheater.

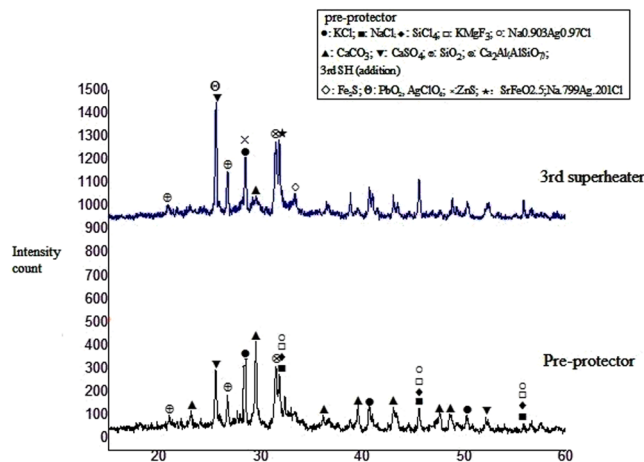


Figure 6. XRD results of deposits from 3rd superheater and pre-protector.

Comparison of the EDS analysis and wet chemical analysis. During the analysis of the deposits by EDS, it was observed that EDS had some shortcomings. The deposit had a depth profile consisting of coarse ash particles on the outer surface while smaller particles inside the particles and in the deposits. This led to a biased chemical composition due to the limited penetration depth of the electron beam. In addition, the EDS analysis is more sensitive to the surface composition of the larger particles than to the average bulk composition. It can also give strong deviations if particles comprise of a surrounding shell which is a property for condensation on solid nuclei³².

In contrast, the wet chemical analysis is a comprehensive technique that prevents all the flaws of the EDS investigation because all particles were considered with a good representation of their mass fractions, the bulk, and also takes into account the whole deposit thickness.

Although data in Figs 3 and 5 are in reasonable agreement, the concentration values of the elements are not the same. The average elemental concentrations from the wet chemical analysis (Fig. 5) are slightly less than those of the EDS analysis (Fig. 3). This was ascribed to the different concentrations of elements with varying depth which affected the average values from the wet chemical analysis. Furthermore, the amounts of large particles containing higher salt concentrations might have been underrepresented in the images investigated by the EDS. It was observed that performing EDS analysis in numerous areas over the entire deposit surface improved the agreement of elemental concentration with the wet chemical analysis method.

XRD deposit analysis. Results from the X-ray diffraction (XRD) analysis of the deposits from the pre-protector and the 3rd superheater are shown in Fig. 6. Deposits of the 3rd superheater showed a large content of PbO and CaSO₄. The observation of calcium sulfate is in contrast with^{26,33}. The possible explanation might be due to the prolonged exposure of the unsulfated CaO in the deposits to the combustion flue gas which may have resulted in the formation of CaSO₄. This explanation is supported by findings of Lai *et al.*³⁴ and Tang *et al.*²⁴ that deposit particles consist of coarse particles rich in O, Ca, S, and C which might be CaSO₄ and calcite (CaCO₃). Furthermore, CaO might have been formed from Ca metal at high oxygen partial pressure and low temperatures over a short period of time^{32,35}.

Even though limited by the deposition selectivity, the deposits contained SiO₂ which may have resulted from the sticking capture and inertial impaction. KCl was present in considerable amounts on the 3rd superheater but was less than CaSO₄. Various types of iron compounds such as Fe₂S and SrFeO₂ were also detected in the 3rd superheater deposits. At pre-protector, the deposit was high in KCl and slight less CaSO₄ as compared to the 3rd superheater. The deposits also contained sorosilicate gehlenite (Ca₂Al(AlSiO₇)) which possibly comes from the solid-state reaction of CaO with Al₂O₃ and SiO₂ at high temperatures³⁶. The deposits on the pre-protector contained large content of calcium carbonate, calcium sulfate, silicon tetrachloride as well as alkali chlorides (KCl and NaCl). Some diffraction peaks were left unidentified, implying that other compounds were probably present in the examined deposits.

Corrosion observation. The morphology of the corroded tube's surface and cross-sectional area for the pre-protector are displayed in Fig. 7. There are many particles of various shapes scattered on the corroded surface of the pre-protector: a spherical-shaped particle (1#) and a rod-shaped particle (2#). From the EDS analysis, it was observed that the spherical-shaped particle is the transition metal chloride. However, only a few spherical-shaped particles were found and most of them were surrounded by the rod-shaped particles, which had a high content of chlorine, sodium, and lead. Particle (2#) was identified as the outer layer of the deposits in terms of structure. This means severe chlorine-induced deposition and further corrosion occurred on the surface of the pre-protector. Therefore, the cross-sectional area of the pre-protector was analyzed vertically and marked as Gap (3#, 4#, and 5#) in Fig. 7(b). It was found that there was a decrease of chlorine content from the outer surface (Gap 3#) to the interface (Gap 5#). This was probably due to the vaporization of iron chloride from the interface to the outer layer during the active oxidation cycle.

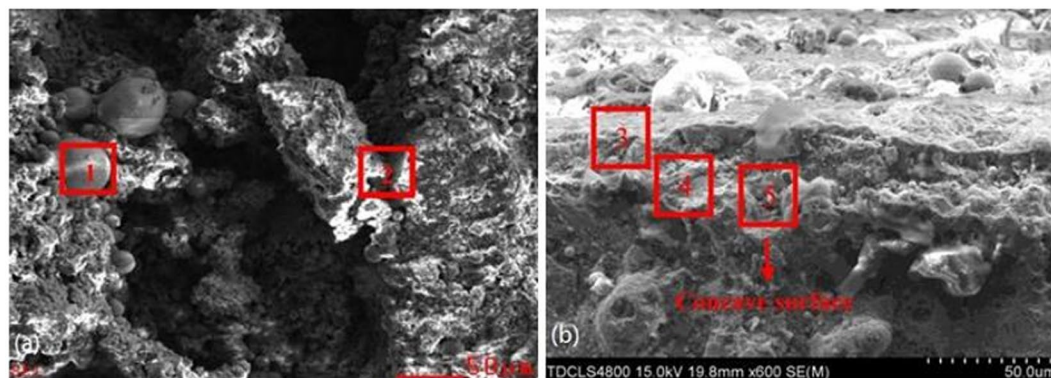


Figure 7. SEM micrograph of (a) pre-protector's surface and (b) cross-sectional area.

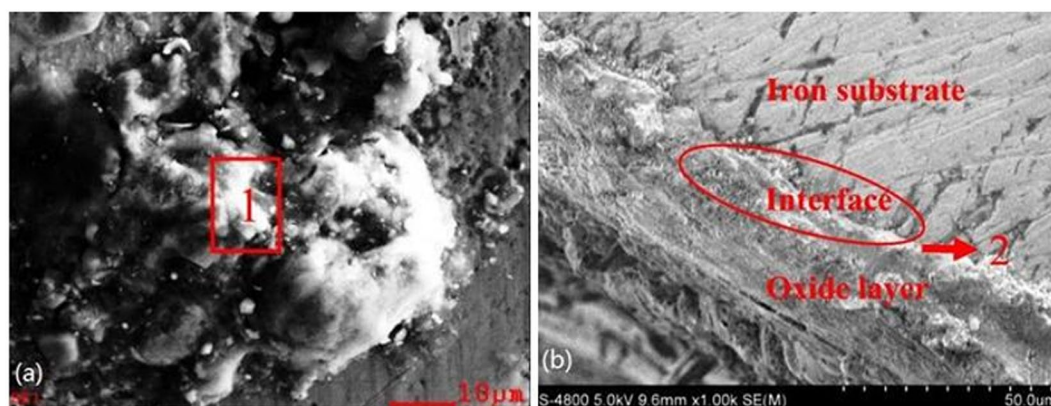


Figure 8. SEM micrograph of (a) 3rd superheater's surface and (b) cross-sectional area.

The slagging surface and cross-section of the 3rd superheater are shown in Fig. 8. From Fig. 8(a), Gap (1#), the massive aggregation of ash deposits was selected and chemically analyzed. The elemental composition of Gap (1#) consisted of a high content of sulfur, sodium, and potassium with lack of calcium and magnesium. In Fig. 8(b), it was visible that the delamination of metal and oxide layer was obvious and the metal/oxide interface was marked as Gap (2#). Some scratches were found scattered in the interface and iron substance. In addition, the chemical composition of Gap (2#) showed that the content of chlorine at the 3rd superheater was slightly less than that at the pre-protector (Gap (5#) in Fig. 7), which proved that the degree of corrosion on the 3rd superheater was less than the pre-protector.

Discussion

The purpose of this study was to investigate the deposit chemistry mainly deposit morphology and concentration of corrosive elements at the pre-protector and the 3rd superheater as well as evaluating their corrosion tendency. The results show that the deposit from both locations had diverse microstructural particles including spherical, elongated, plate-shaped and hemispherical. This observation is consistent with²⁵. Spherical particles could have resulted from the solidification of liquid droplets during cool-down and the other shaped particles might presumably have been emitted from the furnace as solid particles and may have a higher melting point than the spherical particles due to a different chemical composition²⁵. The diversity in the microstructure of the particles was due to the different deposits minerals shown in Fig. 6, which had resulted from the physicochemical reactions that took place during the deposit formation and growth.

The deposit on the 3rd superheater had a large amount of Ca and S while the pre-protector was high in Na, K, Cl, and S indicating the presence of CaSO_4 and a eutectic salt of alkali chloride and sulfate respectively. A large amount of sulfur in deposits was due to the sulfation of alkali chlorides at high steam temperature forming thin and dense alkali sulfates layer at the metal/oxide interface³⁷. Different from the role of calcium sulfate, alkali chlorides especially those in the deposits are more severe than the other species like HCl in the flue gas, due to the formation of eutectic low-melting compounds²⁷. These compounds melt at low temperatures and cause corrosion by forming a flux with the protective oxide layer as well as providing a liquid phase for ionic charge transfer for electrochemical attack⁵.

The detection of more sulfur at the interface than in the outer layer is in strong agreement with literature^{20,38} and it is assumed to be due to sulfation of alkali chloride by SO_3 which might have been catalytically formed within the deposit by the Fe_2O_3 in the oxide layer³⁹. Moreover, it is assumed that SO_2 might have diffused through

the micro-cracks of the oxide layer and reacted with alkali chlorides, which were primarily deposited near the interface forming alkali sulfates⁴⁰.

The pre-protector, which is arranged prior to the 3rd superheater in waste boilers, has higher flue gas temperature (650 °C) leading to an increased surface temperature. The amount of alkali and chlorine in the deposits is high, while that of Ca is lower as shown in Figs 3 and 5. Other ash-forming elements, including aluminum, magnesium, and silicon occurred in minor quantities at all points, but the main elements differed between points. A study by Baxter⁴¹ showed that the deposition mechanisms include condensation, inertial impaction, thermophoresis, eddy impaction and chemical reaction. Liu *et al.*⁴² explained using Johnson-Kendall-Roberts theory that for a general deposition of a particle, a certain critical velocity should be achieved in order for the particle to either rebound or deposit. The particle diameter negatively influences its critical velocity, implying that smaller particles adhere easily to the surface of the boilers⁴². Since the pre-protector has a temperature around 700 °C, the bonding energy between the surface and particle is in this range. This indicates that during the early stage of deposition, thermophoretic and condensation mechanisms of sub-micrometer particles are dominant. When the deposits increase in mass, ash heat-transfer coefficient decreases, resulting in an increase in the ash deposit surface temperature, and subsequently lead to the partial melting of ash deposits at the top layer. For example, K₂SO₄ has a melting point 1069 °C but decreases to 694 °C when reacted with potassium chloride to form eutectic KCl-K₂SO₄⁵. The deposit which is partially melted becomes more adhesive; hence accelerate the impaction of particles. That is why the pre-protector ash deposit formed around 700 °C had high amounts of alkali, S, and Cl. At the 3rd superheater, which is arranged after the pre-protector where the deposition temperature is around 400 °C, a large temperature gradient between the metal temperature and the flue gas exists. This large temperature difference promotes thermophoretic/condensation mechanisms of fine particles. According to Tang *et al.*²⁴, the ultrafine sub-micrometer particles act like “glue” during the ash deposition at lower temperatures. CaO are fine particles and have a large specific surface area, therefore they influence their critical velocity resulting in the large adhesion force to the metal surface which leads to the aggregation of fine CaO particles on heated surfaces, forming ash deposits⁴³. The precipitation and accumulation of fine CaO particles on the 3rd superheater are the reason why more CaSO₄ as binders or as particles were detected in the deposits. CaO and or CaCO₃ acting as a paste between the particles result in the formation of CaSO₄. Sulfates, however, are less corrosive and only play the main role in preventing penetration of gases to the interface³⁹.

The chemical composition of the ash deposits was important to the reveal of the deposition mechanism. SEM analysis shows that the pre-protector deposits consist of thicker and denser particles while the 3rd superheater deposits consist of thinner and fine particles. Based on the composition and morphology of the deposits investigated, this study has taken a step in the understanding of deposit formation at the pre-protector and the 3rd superheater. Chemical composition analysis showed that deposits at the 3rd superheater had high Ca and S compounds, in which calcium-rich compounds in the deposits went through sulfation process. Xu *et al.*⁴⁴ mentioned that the ultrafine sub-micrometer particles act as adhesive agents during deposit formation at low temperatures. Ca compounds (CaO and CaCO₃) released from the MSW fuel, are ultrafine particles and have a large specific surface area, which leads to a large binding force among them. These particles aggregate on the 3rd superheater surfaces through thermophoretic and condensation mechanisms due to a large temperature difference between the metal temperature and the flue gas⁴³. Moreover, condensed elements on this layer result in the formation of a sticky deposit layer in which fly ash particles bond through impaction process. Sulfates largely condense at high temperatures than chlorides and are more thermodynamically favored as temperatures decrease, delaying volatilization at lower temperatures, thus detected in more concentration at the 3rd superheater where the metal temperature is relatively low. KCl-K₂SO₄ is a low melting compound formed from the reaction of KCl and K₂SO₄ in which the later was formed from sulfation of alkali chloride making the deposit more sticky for capturing of fly ash particles⁴⁵.

At the pre-protector, the chemical composition detected suggests a different mechanism. The high temperature of deposit layer makes it easily sintered, and therefore increases the probability of ash particles to bond themselves through inertial impaction²⁴. The alkali metals released in the flue gas as aerosols of sulfates, chlorides, and hydroxide go through mineralogical transformations and chemical reactions²⁴. These aerosols then undergo nucleation, adsorption, condensation thereby grows to form submicrometer ash particles as the flue gas temperature decreases and then stick on the heating surfaces forming an adhesive deposit layer through thermophoresis and turbulent diffusion. Some mineralogical reactions between sulfates, chlorides and the flue gas took place, among which anhydrite calcium phase (CaSO₄) as a matrix likes binding material between the grains was formed^{16,20}. Fly ash particles adhesively bond themselves onto this layer through inertial impaction²¹.

According to Otsuka³¹, the molecular quantity of vapor-condensed NaCl and KCl increased with increasing flue gas temperature between 550–800 °C. This is because KCl and NaCl do not volatilize at lower temperatures due to high binding energy (NaCl 787 kJ/mol, KCl 717 kJ/mol)⁴⁶. As the flue gas temperature continues to increase to ~800 °C, alkali chlorides (NaCl and KCl) volatilize forming a gas rich in chlorine compounds⁴⁶. Therefore, flue gas temperature around pre-protector certainly led to the increase of chlorides on tube deposits, which confirmed that deposits at the pre-protector contained more alkali and chlorine with less Ca and S as shown in Figs 3 and 5. Furthermore, from the corrosion point of view, more chlorine was detected in the deposits of the pre-protector than the 3rd superheater, which proved that pre-protector suffered from severe corrosion as seen in Fig. 7. Notwithstanding the limitations of measuring the corrosion rate, this study suggests that the pre-protector deposits with Cl content ~4.86wt.% corroded the steel more than the 3rd superheater deposits with less Cl ~0.9wt.%. This result is consistent with⁴⁷. They observed that corrosion by superheater tube-deposits was less due to the stability of superheater tube-deposits, where the fusion of salt constituents in the deposits could not take place when heated at 400 °C. The superheater tube-deposits with chlorine <2wt.% is likely to remain solid at 400 °C, and therefore corrosion is reduced⁴⁷. Since chlorine content found in the present study at 3rd superheater where the metal temperature is normally 400 °C is less than 2wt.%, the salts are likely to remain solid reducing

Proximate analysis (wt.%)			LHV (kJ/kg)	Ultimate analysis (wt.%)					
Moisture	Volatile*	Ash		C	H	O*	N	S	Cl
41.76	42.19	16.05	6280	42.38	7.17	47.16	2.13	0.07	1.09

Table 2. Proximate analysis and ultimate analysis of waste in Chengdu (wt.%). *By difference. LHV-Lower heating value.

Nominal capacity	Nominal electricity production	Primary air flow	Secondary air flow	Steam temperature	Steam pressure
600 Tons/day	12 MWe	30~35 × 10 ³ Nm ³ /h	6~8 × 10 ³ Nm ³ /h	400 °C	4 MPa

Table 3. Specifications and operating parameters of the Unit 1 boiler.

corrosion than the pre-protector with higher chlorine content and higher temperature. Moreover, the presences of high sulfur content reduce corrosion by sulfation of alkali chlorides^{37,48}. This might presumably be the reason why the 3rd superheater experienced a lower corrosion than the pre-protector.

As deposition is the driven reason for corrosion, an effective physical way using a weight-driven device for deposit removal to reduce corrosion can be applied in this WIP. The principle of this device is utilizing a small capacity motor as the power to drive a long axis at a low speed. There are many vibration hammers hanging in the long axis beating the heat transfer surface in boilers to let the ash deposit fall off from the tubes. The advantage of mechanical vibration and beating is less power consumption and no additions to the flue gas. But this would not be good for the weld seam strength of the boiler tubes and might lead to the reduction of its service life and also enhanced corrosion-erosion.

Chemical way to reduce chlorine-induced corrosion can be employed by adding sulfate compounds to convert alkali chlorides into less corrosive alkali sulfates and HCl. Vattenfall Company, one of the European's largest generators of electricity and heat, adopts adding ammonium sulfate to waste boilers by the real-time monitoring system. This was already used in a fluidized bed boiler firing biomass in Poland⁴⁹. Moreover, optimizing the combustion environment by reducing the temperature can prevent the deposition of alkali chlorides on the pre-protector while facilitating the formation of calcium sulfates which are less corrosive. Although this approach can reduce the boiler efficiency, the service life of the boiler can be prolonged and reduce the maintenance cost.

Experimental

Materials. Waste samples collected from the Chengdu waste incineration plant were sorted into single fractions and then categorized into three groups: organic, inorganic, and recyclable wastes in order to obtain a better understanding of the waste composition. The organic part consisted mainly of food wastes ~43.63wt.% and grass ~0.99wt.%; inorganic wastes comprised of ashes ~10.91wt.% and bricks ~0.24wt.%; and recyclable part was composed mainly of plastics ~23.52wt.%, papers ~13.12wt.%, textiles ~3.67wt.%, glasses ~3.36 wt.% and metals ~0.55wt.%. The waste samples were tested using an elemental analyzer (Analytik Jena multi[®] EA 2000) for the ultimate analysis shown in Table 2 following the American Standards for Testing and Materials D5373–2008 criterion. The organic part, especially the food residues occupied approximately half of the waste composition which is similar to other Chinese cities⁵⁰. Also, plastics in recyclable part take a large proportion which occupied almost a quarter of the waste composition. Plastics and food residues have been reported as the main source of chlorine (~0.5–1.0wt.%)¹¹, therefore chlorine content was tested following the method described elsewhere¹¹, and thus a chlorine concentration of 1.09% was found (Table 2). The composition of MSW and ultimate analysis were the average values obtained in winter in 2015. Sampling and analysis methods for MSW fuels were based on CJ/T 313–2009 criterion⁵¹.

Plant introduction. Experiments were conducted in a WIP in Chengdu, China. This plant consists of three boilers with the total capacity of 1800 tons per day of MSW collected from three districts in Chengdu. The energy recovery system is designed for power generation and heat net. The Unit I boiler was selected as the tested boiler and its operational parameters are shown in Table 3.

The schematic diagram of this WIP is shown in Fig. 9. During the experiments, there were stable operations and the boiler did not experience any malfunctions. The flue gas passed through the furnace chamber, the secondary burning chamber in the second pass of the boiler, the pre-protector, the tertiary superheater (3rd SH), the secondary superheater (2nd SH), and the primary superheater (1st SH). After primary superheater, the gas passed through the evaporator and three economizers (3rd EC, 2nd EC, and 1st EC). Finally, the fly ash particles were removed in a semi-dry scrubber. Several thermocouples were set near the probes to monitor the flue gas temperature. The steel material used for the pre-protector was 20 G (F-C) and is composed of 0.21% C, 0.5% Mn, 0.27% Si, 0.03% S, 0.03% P, 0.3% Cr and Fe as balance. The ring probes of 20 G samples were cut into 50 mm in length and ground with 800# grit SiC paper. The probes were cleaned and degreased with acetone in an ultrasonic bath and subsequently dried at 105 °C until no weight change. Probes were then set at the pre-protector and the 3rd superheater.

Deposit sampling. After one-year exposure, ash deposit samples were collected from the pre-protector as well as the 3rd superheater and were subsequently stored in airtight containers to exclude atmospheric moisture as some products are hygroscopic. Five samples were collected from the pre-protector and two samples from the 3rd superheater. The ash deposit samples were removed from the tubes in different portions and depth with a knife

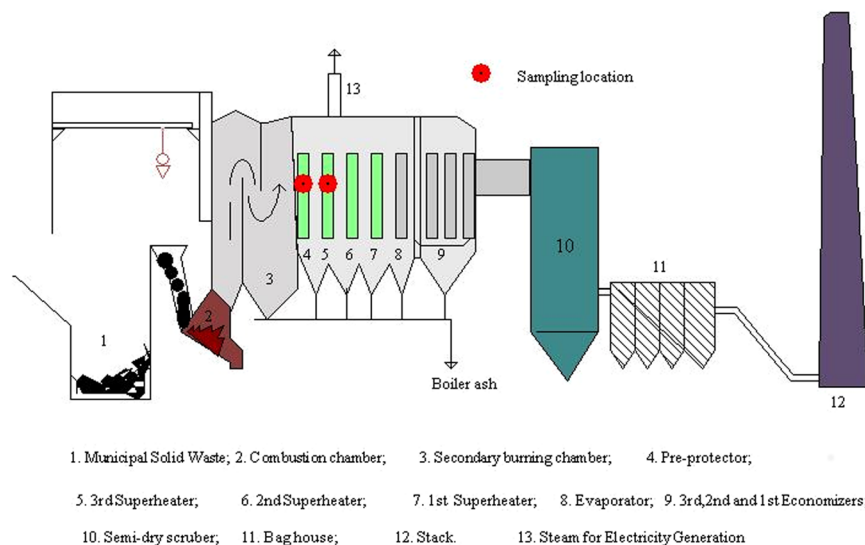


Figure 9. Schematic diagram of the WIP in Chengdu.

in order to find the overall concentrations of K, Na, Cl, S, and Ca in the deposit. The other elements analyzed are shown in the Supplementary information (Supplementary Table S1). In order to determine the chemical composition in terms of the deposit growth on pre-protector, three ash samples of each layer were collected from different locations and mixed forming a composite sample for the outer layer, inner layer, and interface. The deposit sampling was done by collecting ash deposits for the outer layer to a depth of 3 mm on three separate positions, mix them and subject it to wet chemical analysis; then scrape the deposit to the middle layer to collect ash deposits and finally scrape until close to metal to collect samples for the interface. This procedure was done as it gives more accurate amounts of elements than simple EDS, which analyses on small portions. Thereafter, the probes were carefully removed from the pre-protector and the 3rd superheater. They were cut into four pieces and the cross sections were polished and dried for further analyses while preserving the integrity of the deposits in order to investigate the corrosion attack.

Ash deposits analysis. Wet chemical methods were used to analyze the deposits and were done on the windward side of the ring. To determine the concentration of Cl, we have detailed well the procedure in our previous paper¹¹. In the chemical analyses of deposits for calcium concentrations, $\text{Na}_2\text{B}_4\text{O}_7$ was fluxed on the deposits and then analyzed using ICP-AES. Na and K contents were determined by adding lithium borate to the deposits and then analyzed using Atomic Absorption Spectroscopy. Sulfur contents were obtained by iodine titration. These procedures were done to determine the actual quantities of K, Cl, Na, Ca, and S coming from the flue gas that was deposited on the pre-protector and the 3rd superheater and also determines their concentrations in terms of deposit growth on pre-protector.

In addition, the morphology of the deposit surface was analyzed using scanning electron microscopy (SEM) (Philips XL-30 TMP ESEM, 20 kV, Holland). The images obtained were supplemented by EDS analysis for comparison with wet chemical methods. Furthermore, the ash deposits from both locations were ground, passed through a sieve with a mesh size of 70 mm and were stored in desiccators. X-ray Diffraction (XRD) study was then conducted to determine the crystalline compositions in the deposits using a Phillips X-pert X-ray diffraction system with $\text{CuK}\alpha$ radiation.

Data availability. All data generated and analyzed during this study are included in this published article. Raw wet chemical analysis data used to plot Fig. 5 are provided in Supplementary Table S1.

Conclusion

Municipal solid waste incineration results in severe deposition and corrosion in WIP. Troublesome elements to these problems include K, Na, Cl, Ca, and S. A comparative investigation of deposit chemistry and corrosion of the pre-protector and the 3rd superheater at a 36 MWe WIP showed that; the deposits from the pre-protector are rich in Cl, K, and Na while deposit from the 3rd superheater contains more Ca and S. The concentration of alkali decreased from the interface to the outer layer while Cl increased in the same direction in deposits at the pre-protector. The concentration of Ca and S increased from the outer layer of the deposits to the interface while alkali decreased in the same trend in the deposits at the 3rd superheater. The deposit formation at the pre-protector was mainly influenced by alkali chlorides while at the 3rd superheater by ultrafine sub-micrometer Ca-rich compounds. Based on the deposits element composition and corrosion of the metal samples, we conclude that pre-protector ash deposits are more severe than the 3rd superheater ash deposits. However, the interaction of alkali metals and chlorine in corrosion warrant further research.

References

- Tang, X., Jin, Y., McLellan, B. C., Wang, J. & Li, S. China's coal consumption declining-impermanent or permanent? *Resources, Conservation and Recycling*. <https://doi.org/10.1016/j.resconrec.2016.1007.1018> (2016).
- Yuan, J. The future of coal in China. The review. *Resources, Conservation and Recycling*. <https://doi.org/10.1016/j.resconrec.2016.1012.1006> (2016).
- Al-Hamamre, Z. *et al.* Wastes & biomass materials as sustainable-renewable energy resources for Jordan. *Renewable and Sustainable Energy Reviews*. **67**, 295–314 (2017).
- Na-Yang, H. Z., Chen, M., Shao, L.-M. & He, P.-J. Greenhouse gas emissions from MSW incineration in China: impacts of waste characteristics and energy recovery. *Waste Management*. **32**(12), 2552–2560 (2012).
- Niu, Y., Tan, H. & Hui, S. Ash-related issues during biomass combustion: Alkali-induced slagging, silicate melt-induced slagging (ash fusion), agglomeration, corrosion, ash utilization, and related countermeasures. *Progress in Energy and Combustion Science*. **52**, 1–61 (2016).
- National-Bureau-of-Statistics-of-China. *China Statistical Yearbook*, China Statistical Press Beijing, China, (2011).
- National-bureau-of-statistics-of-China. *China statistical yearbook*, China Statistics Press. Beijing, (2012).
- IEA. Renewable electricity generation climbs to second place after coal, International Energy Agency. (2013).
- National-Development-and-Reform-Comission. Mid-long term development plan for renewable energy. *Renew Energy Resour.* **25**, 1–5 (2007).
- Albina, D. O., Millrath, K. & Themelis, N. J. In *Effects of feed composition on boiler corrosion in waste-to-energy plants*, 12th North American waste-to-energy conference, Savannah, Georgia, USA, 2004.
- Ma, W., Hoffmann, G., Schirmer, M., Chen, G. & Rotter, V. S. Chlorine characterization and thermal behavior in MSW and RDF. *J Hazard Mater.* **178**, 489–498 (2010).
- Niu, Y. *et al.* Investigations on biomass slagging in utility boiler: Criterion numbers and slagging growth mechanisms. *Fuel Processing Technology*. **128**, 499–508 (2014).
- Martin, J. J.-E., Koralewska, R. & Wohlleben, A. Advanced solutions in combustion-based WtE technologies. *Waste Manage.* **37**, 147–156 (2015).
- Michelsen, H. P., Larsen, O. H., Frandsen, F. J. & Dam-Johansen, K. In *Deposition and high temperature corrosion in a 10 MW straw fired boiler.*, Proceedings of engineering foundation conference on biomass usage for utility and industrial power, Snowbird, Utah, April 28-May 3, 1996; Snowbird, Utah, 1996.
- Montejo, C., Costa, C., Ramos, P. & Márquez, M. C. Analysis and comparison of municipal solid waste and reject fraction as fuels for incineration plants. *Appl Therm Eng.* **31**, 2135–2140 (2011).
- Phongphiphat, A. *et al.* Investigation into high-temperature corrosion in a large-scale municipal waste-to-energy plant. *Corros. Sci.* **52**(12), 3861–3874 (2010).
- Bashir, M. S. *et al.* Ash transformation and deposit build-up during biomass suspension and grate firing: full-scale experimental studies. *Fuel Process Technol* **97**, 93–106 (2012).
- Skrifvars, B. J., Backman, R., Hupa, M., Salmenoja, K. & Vakkilainen, E. Corrosion of superheater steel materials under alkali salt deposits e part 1: the effect of salt deposit composition and temperature. *Corros. Sci.* **50**(5), 1274–1282 (2008).
- Phongphiphat, A., Ryu, C., Finney, K. N., Sharifi, V. N. & Swithenbank, J. Ash deposit characterisation in a large-scale municipal waste-to-energy incineration plant. *J Hazard Mater.* **186**, 218–226 (2011).
- Chen, G., Zhang, N., Ma, W., Rotter, V. S. & Wang, Y. Investigation of chloride deposit formation in a 24 MWe waste to energy plant. *Fuel*. **140**, 317 (2015).
- Reichelt, J., Pfrang, G., Bergfeldt, B., Seifert, H. & Knapp, P. Formation of ash deposits on the surfaces of superheaters and economisers of MSW incinerator plants. *Waste Manage.* **33**, 43–51 (2013).
- Bankiewicz, D., Enestam, S., Yrjas, P. & Hupa, M. Experimental studies of Zn and Pb induced high temperature corrosion of two commercial boiler steels. *Fuel Process Technol.* **105**(1), 89–97 (2013).
- Pfrang-Stotz, G., Reichelt, J., Bergfeldt, B. & Seifert, H. Systematic Investigation of deposits in the boiler of a semi-technical rotary kiln incinerator: mineralogical and chemical characterization. *Environ Eng Sci.* **24**, 1190–1200 (2006).
- Tang, Z. *et al.* Experimental investigation of ash deposits on convection heating surfaces of a circulating fluidized bed municipal solid waste incinerator. *Journal of environmental science.* **48**, 169–178 (2016).
- Thiel, C., Pohl, M., Grahl, S. & Beckmann, M. Characterization of mineral matter particles in gasification and combustion processes. *Fuel*. **152**, 88–95 (2015).
- Schumacher, S. *et al.* Particle sampling in boilers of waste incineration plants for characterizing corrosion relevant species. *Corrosion Science.* **110**, 82–90 (2016).
- Uusitalo, M. A., Vuoristo, P. M. J. & Mantyla, T. A. High temperature corrosion of coatings and boiler steels below chlorine-containing salt deposits. *Corrosion Science.* **46**, 1311–1331 (2004).
- Niu, Y. *et al.* Slagging Characteristics on the Superheaters of a 12 MW Biomass-Fired Boiler. *Energy Fuels.* **24**, 5222–5257 (2010).
- Zbogar, A., Frandsen, F., Jensen, P. A. & Glarborg, P. Shedding of ash deposits. *Progress in Energy and Combustion Science.* **35**, 31–56 (2009).
- Kawahara, Y. High temperature corrosion mechanisms and effect of alloying elements for materials used in waste incineration environment. *Corrosion Science.* **44**, 223–245 (2002).
- Otsuka, N. A thermodynamic approach on vapor-condensation of corrosive salts from flue gas on boiler tubes in waste incinerators. *Corros. Sci.* **50**(6), 1627–1636 (2008).
- Schumacher, S. *et al.* An artifact-minimizing method for total dust sampling and chemical characterization of industrial high-temperature aerosols. *Aerosol Science and Technology.* <https://doi.org/10.1080/02786826.02782017.01330534> (2017).
- Deuerling, C. F., Maguhn, J., Nordsieck, H. O., Warnecke, R. & Zimmermann, R. Measurement System for Characterization of Gas and Particle Phase of High Temperature Combustion Aerosols. *Aerosol Science and Technology.* **44**(1), 1–9 (2010).
- Lai, Z., Ma, X., Tang, Y., Li, M. & Ni, J. Deposit analysis of water-wall tubes in a municipal solid waste grate incinerator. *Applied Thermal Engineering.* **66**, (2014).
- Brunner, T., Fluch, J., Obernberger, I. & Warnecke, R. Investigations of aerosol formation pathways during MSW combustion based on high-temperature impactor measurements. *Fuel Processing Technology.* **105**, 154–160 (2013).
- Unsworth, J. F., Barratt, D. J., Park, D. & Titchener, K. J. Ash formation during pulverized coal combustion: 2. *The significance of crystalline anorthite in boiler deposits.* *Fuel* **67**, 632–641 (1988).
- Andersson, S. *et al.* Sulfur recirculation for increased electricity production in Waste-to-Energy plants. *Waste Manage.* **34**, 67–78 (2014).
- Åmand, L. E., Leckner, B., Eskilsson, D. & Tullin, C. Deposits on heat transfer tubes during co-combustion of biofuels and sewage sludge. *Fuel.* **85**(10–11), 1313–1322 (2006).
- Nielsen, H. P., Frandsen, F. J., Dam-Johansen, K. & Baxter, L. L. The implications of chlorine-associated corrosion on the operation of biomass-fired boilers. *Prog. Energy Combust* **26**(3), 283–298 (2000).
- Montgomery, M., Vilhelmsen, T. & Jensen, S. A. Potential high temperature corrosion problems due to co-firing of biomass and fossil fuels. *Materials and Corrosion.* **59**(10), 783–793 (2008).
- Baxter, L. L. Ash deposition during biomass and coal combustion: a mechanistic approach. *Biomass Bioenergy* **4**, 85–102 (1993).

42. Liu, G., Li, S. & Yao, Q. A JKR-based dynamic model for the impact of micro-particle with a flat surface. *Powder Technol.* **207**, 215–223 (2011).
43. Kanaoka, C., Hata, M. & Makino, H. Measurement of adhesive force of coal flyash particles at high temperatures and different gas compositions. *Powder Technol.* **118**, 107–112 (2001).
44. Xu, X., Li, S., Li, G. & Yao, Q. Effect of co-firing straw with two coals on the ash deposition behavior in a down-fired pulverized coal combustor. *Energy Fuel* **24**(1), 241–249 (2010).
45. Brostrom, M. *et al.* Sulfation of corrosive alkali chlorides by ammonium sulfate in a biomass fired CFB boiler. *Fuel Processing Technology.* **88**(11–12), 1171–1177 (2007).
46. Yudovich, Y. E. & Ketris, M. P. Chlorine in coal: A review. *International Journal of Coal Geology.* **67**, 127–144 (2006).
47. Otsuka, N. Chemistry and melting characteristics of fireside deposits taken from boiler tube in waste incinerators. *Corrosion Science.* **53**, 2269–2276 (2011).
48. Andersson, C., inventor; Vattenfall AB (publ), assignee. Method for operating a heat-producing plant for burning chlorine-containing fuels. European Patent EP 1354167. 2002 August 01.
49. Yin, C., Rosendahl, L. A. & Kaer, S. K. Grate-firing of biomass for heat and power production. *Prog Energy Combust.* **34**(6), 725–754 (2008).
50. Zhou, H., Meng, A., Long, Y., Li, Q. & Zhang, Y. An overview of characteristics of municipal solid waste fuel in China: Physical, chemical composition and heating value. *Renew Sust Energy Rev* **36**(30), 107–122 (2014).
51. Chinese-standards. Sampling and analysis methods for domestic waste. <http://www.chinesestandard.net/List-PDF/MISC.aspx?PageNumber=25>. Accessed 12/10/15.

Acknowledgements

The authors are thankful to National High Technology Support Project of China (Grant No. 2014BAC02B03), High Technology Support Project of Tianjin (16PTGCCX00170, 16YFXTSF00540, 13ZCZDSF00900), Tianjin Research Program of Application and Advanced Technology (15JCQNJC06600).

Author Contributions

W.M., T.W., G.C. and N.Z. designed the experimental research. W.M., T.W., N.Z., Z.Z. and X.W. conducted samples collection and analysis. T.W., N.Z., Y.B. and Z.Z. prepared tables and Figures. W.M., T.W. and N.Z. wrote the manuscript. All authors reviewed the manuscript.

Additional Information

Supplementary information accompanies this paper at <https://doi.org/10.1038/s41598-017-17438-3>.

Competing Interests: The authors declare that they have no competing interests.

Publisher's note: Springer Nature remains neutral with regard to jurisdictional claims in published maps and institutional affiliations.



Open Access This article is licensed under a Creative Commons Attribution 4.0 International License, which permits use, sharing, adaptation, distribution and reproduction in any medium or format, as long as you give appropriate credit to the original author(s) and the source, provide a link to the Creative Commons license, and indicate if changes were made. The images or other third party material in this article are included in the article's Creative Commons license, unless indicated otherwise in a credit line to the material. If material is not included in the article's Creative Commons license and your intended use is not permitted by statutory regulation or exceeds the permitted use, you will need to obtain permission directly from the copyright holder. To view a copy of this license, visit <http://creativecommons.org/licenses/by/4.0/>.

© The Author(s) 2017